

---

This is an electronic reprint of the original article.  
This reprint may differ from the original in pagination and typographic detail.

Tiitinen, Lauri; Hinkkanen, Marko; Harnefors, Lennart

## Stable and Passive Observer-Based V/Hz Control for Induction Motors

*Published in:*  
2022 IEEE Energy Conversion Congress and Exposition (ECCE)

*DOI:*  
[10.1109/ECCE50734.2022.9948057](https://doi.org/10.1109/ECCE50734.2022.9948057)

Published: 13/10/2022

*Document Version*  
Peer-reviewed accepted author manuscript, also known as Final accepted manuscript or Post-print

*Published under the following license:*  
CC BY

*Please cite the original version:*  
Tiitinen, L., Hinkkanen, M., & Harnefors, L. (2022). Stable and Passive Observer-Based V/Hz Control for Induction Motors. In *2022 IEEE Energy Conversion Congress and Exposition (ECCE)* (pp. 1-8). Article 9948057 (IEEE Energy Conversion Congress and Exposition). IEEE. <https://doi.org/10.1109/ECCE50734.2022.9948057>

---

This material is protected by copyright and other intellectual property rights, and duplication or sale of all or part of any of the repository collections is not permitted, except that material may be duplicated by you for your research use or educational purposes in electronic or print form. You must obtain permission for any other use. Electronic or print copies may not be offered, whether for sale or otherwise to anyone who is not an authorised user.

# Stable and Passive Observer-Based V/Hz Control for Induction Motors

Lauri Tiitinen  
Aalto University  
Espoo, Finland  
lauri.tiitinen@aalto.fi

Marko Hinkkanen  
Aalto University  
Espoo, Finland  
marko.hinkkanen@aalto.fi

Lennart Harnefors  
ABB Corporate Research  
Västerås, Sweden  
lennart.harnefors@se.abb.com

**Abstract**—This paper proposes an observer-based volts-per-hertz (V/Hz) control method for induction motors. The proposed method consists of a state-feedback control law and a flux observer, both of which are designed to be inherently sensorless. The gains can be selected using simple closed-form expressions, resulting in a locally stable and passive system in the whole feasible operating range. Unstable regions and heuristic tuning of conventional V/Hz control are thus avoided. Compared to sensorless field-oriented control, no speed controller or separate field-weakening method is needed, the full inverter voltage can be utilized, and the sensitivity to parameter errors is reduced.

**Index Terms**—Induction machine, observer, scalar control, sensorless, stability, volts-per-hertz (V/Hz) control

## I. INTRODUCTION

Volts-per-hertz (V/Hz) control of induction motors may suffer from the stability problems at low speeds under heavy loads as well as at medium speeds under low loads [1], [2]. To reduce these unstable regions and to increase damping, conventional V/Hz control methods include a compensator based on the measured stator current [2]–[4], as exemplified in Fig. 1(a). The stability and control performance depends on the compensator, whose structure is typically heuristic and tuning is based on trial-and-error methods. Parametrization of the V/Hz curve including the stator resistance voltage drop (RI) compensation can also be cumbersome. Conventional V/Hz control methods cannot completely remove the unstable regions, even if perfect RI compensation is assumed [2].

Contrary to V/Hz control, sensorless field-oriented control methods are based on the dynamic motor model. If the flux observer is well designed and if the motor parameters are known, the local stability in the whole feasible operating range—referred to as the *complete stability*—can be achieved [5], [6]. However, in many applications, the mechanical subsystem is unknown and its identification is impractical, which complicates tuning of the speed controller. Sensorless field-oriented control can also be sensitive to parameter errors. For operating at high speeds, a specific field-weakening algorithm is needed. Typically, the full inverter voltage is not available in the steady state, since the current controller needs some voltage reserve.

This work was supported in part by ABB Oy and in part by the Academy of Finland Centre of Excellence in *High-Speed Electromechanical Energy Conversion Systems*.

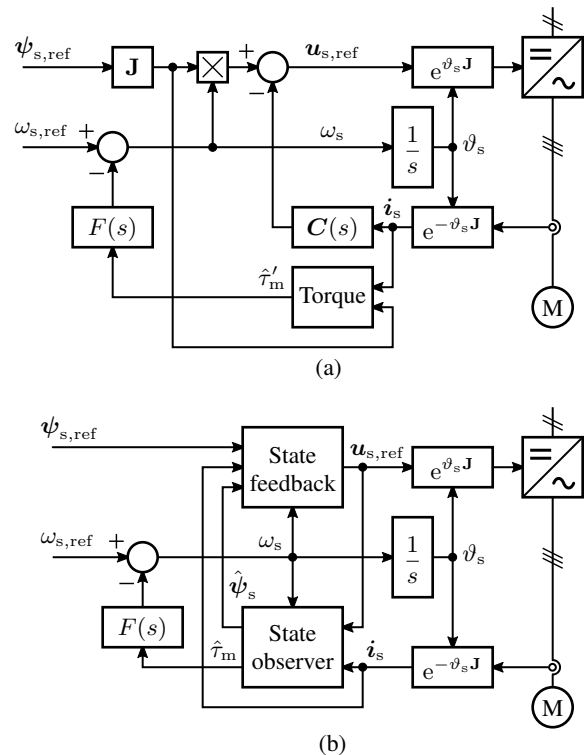


Fig. 1. V/Hz control: (a) conventional; (b) proposed. In (a),  $C(s)$  is a lead-lag compensator resulting from parallel connection of RI compensation and high-pass filtering for damping improvement, and  $\hat{\tau}'_m$  is a torque estimate (cf. Appendix A). In (b), the state feedback is defined in (5) [or (6)] and the observer in (11). In both,  $F(s)$  is the high-pass filter (8).

This paper proposes an observer-based V/Hz control, shown in Fig. 1(b), which aims to combine the best features of V/Hz control and sensorless field-oriented control. The proposed method consists of a state-feedback control law and a flux observer, both of which are designed to be inherently sensorless, enabling the local stability and passivity in every feasible operating point. As compared to conventional V/Hz control, the heuristic compensator is replaced with the observer. As compared to sensorless field-oriented control, neither speed controller nor separate field-weakening method is needed, the full inverter voltage can be utilized, and the sensitivity to the parameter errors is reduced.

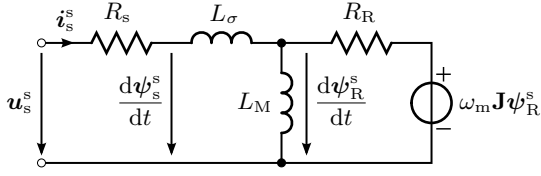


Fig. 2. Equivalent circuit of the induction motor in stator coordinates (where vectors are marked with the superscript s).

## II. MOTOR MODEL

The stator current is represented by a column vector  $\mathbf{i}_s = [i_{sd}, i_{sq}]^T$ , where  $i_{sd}$  and  $i_{sq}$  are the d- and q-axis components, respectively, and the superscript T marks the transpose. Other vector quantities are represented similarly. Furthermore, the identity matrix  $\mathbf{I} = \begin{bmatrix} 1 & 0 \\ 0 & 1 \end{bmatrix}$ , the orthogonal rotation matrix  $\mathbf{J} = \begin{bmatrix} 0 & -1 \\ 1 & 0 \end{bmatrix}$ , and the zero matrix  $\mathbf{0} = \begin{bmatrix} 0 & 0 \\ 0 & 0 \end{bmatrix}$  are used in the following equations.

### A. Nonlinear Dynamic Model

The induction motor is modeled using the standard inverse- $\Gamma$  model [7], whose equivalent circuit is shown in Fig. 2. With the stator current  $\mathbf{i}_s$  and the rotor flux linkage  $\psi_R$  as the state variables, the corresponding nonlinear state equations in a coordinate system rotating at the angular speed  $\omega_s$  are

$$L_\sigma \frac{d\mathbf{i}_s}{dt} = -(R_\sigma \mathbf{I} + \omega_s L_\sigma \mathbf{J}) \mathbf{i}_s + (\alpha \mathbf{I} - \omega_m \mathbf{J}) \psi_R + \mathbf{u}_s \quad (1a)$$

$$\frac{d\psi_R}{dt} = R_R \mathbf{i}_s - [\alpha \mathbf{I} + (\omega_s - \omega_m) \mathbf{J}] \psi_R \quad (1b)$$

where  $R_\sigma = R_s + R_R$  is the total resistance and  $\alpha = R_R/L_M$  is the inverse rotor time constant. In addition to  $\omega_s$ , the stator voltage  $\mathbf{u}_s$  and the electrical angular speed  $\omega_m$  are the input variables of this nonlinear system. The stator flux linkage  $\psi_s$  and the electromagnetic torque  $\tau_m$  are selected as the output variables, i.e.,

$$\psi_s = L_\sigma \mathbf{i}_s + \psi_R \quad (1c)$$

$$\tau_m = \mathbf{i}_s^T \mathbf{J} \psi_R \quad (1d)$$

where per-unit (p.u.) quantities are assumed in the torque equation. It can be seen that the torque is nonlinear in the state variables.

A rigid mechanical system is governed by

$$J_m \frac{d\omega_m}{dt} = \tau_m - \tau_L \quad (2)$$

where  $J_m$  is the total moment of inertia and  $\tau_L$  is the load torque. For simplicity, this mechanical system is used as an example in the following analysis, but the stability results are valid for any passive mechanical systems, including resonant mechanics.

### B. Steady-State Operating Point

The nonlinear model (1) can be linearized about the operating point in order to analyze its local stability, cf. Appendix B.

The first step in this linearization process is to solve the steady-state operating point by substituting  $d/dt = 0$ . As an example, the stator current in the steady state is obtained from (1b),

$$\mathbf{i}_{s0} = \frac{\alpha \mathbf{I} + \omega_{r0} \mathbf{J}}{R_R} \psi_{R0} \quad (3)$$

where  $\omega_{r0} = \omega_{s0} - \omega_{m0}$  is the angular slip frequency and the operating-point quantities are marked with the subscript 0. Further, applying (1c) and (3) yields the steady-state relation between the rotor and stator fluxes,

$$\psi_{R0} = \frac{R_R}{L_\sigma} (\omega_{rb} \mathbf{I} + \omega_{r0} \mathbf{J})^{-1} \psi_{s0} \quad (4)$$

where  $\omega_{rb} = (1/L_M + 1/L_\sigma) R_R$  is the breakdown slip frequency. Other steady-state relations can be obtained similarly.

## III. CONTROL SYSTEM

Fig. 1(b) shows the proposed control system. Its core consists of a state-feedback control law and a reduced-order observer, both of which are designed to be inherently sensorless. These two blocks make it possible to stabilize and passivate the motor in its whole feasible operating range. Furthermore, the damping of the mechanical system can be increased using additional feedback from the electromagnetic torque estimate  $\hat{\tau}_m$  through a high-pass filter  $F(s)$ . The control system is described in detail in the following.

### A. State-Feedback Control

The voltage reference for the inverter can be calculated as

$$\mathbf{u}_{s,\text{ref}} = R_s \mathbf{i}_s + \omega_s \mathbf{J} \psi_{s,\text{ref}} + \mathbf{K} (\psi_{s,\text{ref}} - \hat{\psi}_s) \quad (5)$$

where  $\omega_s$  is the stator angular frequency signal,  $\psi_{s,\text{ref}} = [\psi_{s,\text{ref}}, 0]^T$  is an external stator flux reference (that can be kept constant),  $\hat{\psi}_s$  is the stator flux estimate provided by an observer, and  $\mathbf{K}$  is a  $2 \times 2$  gain matrix. This control law is a special case of state-feedback control. Since no rotor speed (or its estimate) appears in the control law, it is *inherently sensorless* [8].

The control law (5) can be rewritten in an alternative form that has some practical merits. Since the reduced-order flux observer is used,  $\hat{\psi}_s = \hat{\psi}_R + L_\sigma \mathbf{i}_s$  holds. Therefore, (5) can be equivalently presented as

$$\mathbf{u}_{s,\text{ref}} = R_s \mathbf{i}_s + \omega_s \mathbf{J} \psi_{s,\text{ref}} + L_\sigma \mathbf{K} (\mathbf{i}_{s,\text{ref}} - \mathbf{i}_s) \quad (6a)$$

$$\mathbf{i}_{s,\text{ref}} = \frac{\psi_{s,\text{ref}} - \hat{\psi}_R}{L_\sigma} \quad (6b)$$

where  $\mathbf{i}_{s,\text{ref}}$  is an intermediate stator current reference. This intermediate signal can be saturated in order to limit the stator current.

### B. Stator Frequency

The internal stator frequency reference can be selected as

$$\omega_s = \omega_{s,\text{ref}} - k_\omega (\hat{\tau}_m - \hat{\tau}_{mf}) \quad (7a)$$

where  $\omega_{s,\text{ref}}$  is an external rate-limited stator frequency reference,  $\hat{\tau}_m$  is the torque estimate, and  $k_\omega$  is a positive gain for

increasing the damping. The signal  $\hat{\tau}_{mf}$  is a low-pass-filtered torque estimate,

$$\frac{d\hat{\tau}_{mf}}{dt} = \alpha_f (\hat{\tau}_m - \hat{\tau}_{mf}) \quad (7b)$$

where  $\alpha_f$  is the bandwidth of the filter. Equivalently, the stator frequency signal can be expressed as

$$\omega_s = \omega_{s,ref} - \underbrace{\frac{k_\omega s}{s + \alpha_f}}_{F(s)} \hat{\tau}_m \quad (8)$$

where  $s = d/dt$  is the differential operator and the operator  $F(s)$  can be recognized as a high-pass filter.

Optionally, a slip compensation scheme can be easily integrated into the proposed method. In this case, the stator frequency reference  $\omega_{s,ref}$  is the sum of an external speed reference  $\omega_{m,ref}$  and a low-pass-filtered slip frequency estimate,

$$\omega_{s,ref} = \omega_{m,ref} + \frac{\alpha_r}{s + \alpha_r} \hat{\omega}_r \quad (9)$$

where  $\alpha_r$  is the bandwidth of the low-pass filter. The instantaneous slip frequency estimate is obtained from the observed quantities as

$$\hat{\omega}_r = \frac{R_R \hat{\tau}_m}{\|\hat{\psi}_R\|^2} \quad (10)$$

If the slip compensation is enabled, the complete stability of the proposed method may not be guaranteed, since the resultant filter consisting of (8)–(10) is generally not passive, unlike the high-pass filter in (8). However, if the bandwidth  $\alpha_r$  is low, the slip compensation does not affect the stability.

### C. Reduced-Order Flux Observer

To be able to apply state-feedback control in (5), the stator (or rotor) flux linkage has to be estimated. The simplest option is to use a reduced-order flux observer [9]. Based on (1b), the reduced-order flux observer can be formulated as [6]

$$\begin{aligned} \frac{d\hat{\psi}_R}{dt} &= \mathbf{u}_{s,ref} - (R_s \mathbf{I} + \omega_s L_\sigma \mathbf{J}) \mathbf{i}_s \\ &\quad - L_\sigma \frac{d\mathbf{i}_s}{dt} - \omega_s \mathbf{J} \hat{\psi}_R + \mathbf{K}_o \mathbf{e} \end{aligned} \quad (11a)$$

where  $\mathbf{K}_o$  is a  $2 \times 2$  observer gain matrix. The output equations are

$$\hat{\psi}_s = \hat{\psi}_R + L_\sigma \mathbf{i}_s \quad (11b)$$

$$\hat{\tau}_m = \mathbf{i}_s^T \mathbf{J} \hat{\psi}_R \quad (11c)$$

The correction vector obtained from (1a) is

$$\mathbf{e} = L_\sigma \frac{d\mathbf{i}_s}{dt} + (R_\sigma \mathbf{I} + \omega_s L_\sigma \mathbf{J}) \mathbf{i}_s - (\alpha \mathbf{I} - \hat{\omega}_m \mathbf{J}) \hat{\psi}_R - \mathbf{u}_{s,ref} \quad (11d)$$

where  $\hat{\omega}_m$  is the speed estimate. The speed can be estimated by integrating the component of the correction vector  $\mathbf{e}$  orthogonal to the rotor flux estimate, i.e., [5]

$$\frac{d\hat{\omega}_m}{dt} = \alpha_o \frac{\hat{\psi}_R^T \mathbf{J} \mathbf{e}}{\|\hat{\psi}_R\|^2} \quad (11e)$$

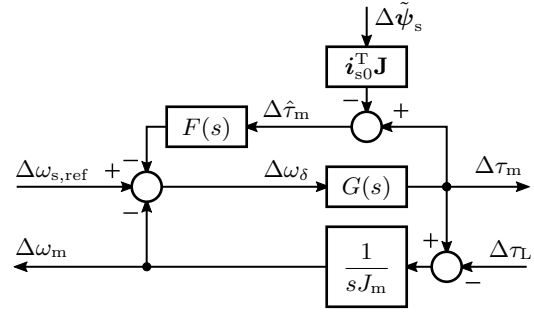


Fig. 3. Linearized closed-loop system resulting from the proposed control system. The flux estimation error  $\Delta\psi_s$  is decoupled from the mechanical dynamics. The transfer function  $G(s)$  and the high-pass filter  $F(s)$  defined in (8) are passive. Therefore, the whole closed-loop system is passive (and stable) for any passive mechanical subsystems.

where  $\alpha_o$  is the speed-estimation bandwidth.

As special cases,  $\mathbf{K}_o = \mathbf{0}$  yields the voltage model and  $\mathbf{K}_o = \mathbf{I}$  yields the current model. The flux observer in (11a) becomes inherently sensorless if the observer gain fulfills the condition  $\mathbf{K}_o \mathbf{J} \hat{\psi}_R = \mathbf{0}_{2,1}$ , i.e., the speed-dependent term in (11d) disappears. A general inherently sensorless stabilizing gain, allowing arbitrary pole placement for the linearized estimation-error dynamics, is available [6]. Here, its special case is used

$$\mathbf{K}_o = \frac{2\sigma_o(\alpha \mathbf{I} + \hat{\omega}_m \mathbf{J}) \hat{\psi}_R \hat{\psi}_R^T}{\alpha^2 + \hat{\omega}_m^2} \frac{1}{\|\hat{\psi}_R\|^2} \quad (12)$$

where  $\sigma_o$  the desired exponential decay rate of the estimation error. The speed estimate  $\hat{\omega}_m$  is needed only in the observer gain (12). If the stability at low speeds in the regenerating mode is not required, the observer gain can be simplified by replacing  $\hat{\omega}_m$  with  $\omega_{s,ref}$ , making the speed estimation (11e) unnecessary.<sup>1</sup>

## IV. ANALYSIS

The local stability and passivity of the proposed control method, shown in Fig. 1(b), are analyzed by means of small-signal linearization. For simplicity, the inverter is assumed to be ideal,  $\mathbf{u}_s = \mathbf{u}_{s,ref}$ , and parameter errors are omitted. The small-signal deviation of the stator current about the operating point is denoted by  $\Delta\mathbf{i}_s = \mathbf{i}_s - \mathbf{i}_{s0}$  and other small-signal variables are marked similarly. With no loss of generality, the signals and systems are expressed in the Laplace domain in the following analysis. The derivation of the following transfer functions are presented in detail in Appendix B.

### A. Stator Flux Dynamics

State-feedback control (5) allows to shape the closed-loop stator-flux dynamics,  $\Delta\psi_s(s) = \mathbf{G}_c(s)\Delta\psi_{s,ref}(s)$ . For conve-

<sup>1</sup>For inherently sensorless gains, the speed estimator in (11e) is identical with the expression  $d\hat{\omega}_m/dt = \alpha_o(\hat{\omega}_s - \hat{\omega}_r - \hat{\omega}_m)$ , where  $\hat{\omega}_s$  is the angular speed of the rotor flux estimate. The estimator (11e) is independent of coordinates and simple to implement, since the correction vector  $\mathbf{e}$  is already available.

nience, the gain matrix of the form  $\mathbf{K} = \sigma_c \mathbf{I} + (\omega_d - \omega_{s0}) \mathbf{J}$  is considered, yielding

$$\mathbf{G}_c(s) = \frac{(\sigma_c s + \sigma_c^2 + \omega_d^2) \mathbf{I} + \omega_d s \mathbf{J}}{(s + \sigma_c)^2 + \omega_d^2} \quad (13)$$

where  $\sigma_c$  is the exponential decay rate and  $\omega_d$  is the damped natural frequency, respectively. It can be seen that the poles  $s = -\sigma_c \pm j\omega_d$  can be placed arbitrarily by means of the two gains  $\sigma_c$  and  $\omega_d$ . Furthermore, the stator-flux dynamics in (13) are decoupled from the rotor-flux dynamics, which indicates that the harmful coupling between the stator and rotor electrical dynamics, appearing in conventional V/Hz control [2], is avoided. The dynamics in (13) also reveal that the motor can be magnetized without any special algorithms, simply using a constant stator flux reference.

### B. Mechanical Dynamics

Fig. 3 shows a block diagram of the resulting closed-loop mechanical dynamics. The transfer functions are presented in detail in Appendix B. It is also shown there that the separation principle holds for the linearized system, which allows the control and observer dynamics to be designed separately. The transfer function from  $\Delta\omega_\delta(s) = \Delta\omega_s(s) - \Delta\omega_m(s)$  to the electromagnetic torque  $\Delta\tau_m(s)$  is

$$G(s) = \frac{\Delta\tau_m(s)}{\Delta\omega_\delta(s)} = \frac{\psi_{R0}^2 \omega_{rb} s + \omega_{rb}^2 - \omega_{r0}^2}{R_R (s + \omega_{rb})^2 + \omega_{r0}^2} \quad (14)$$

where  $\psi_{R0} = \|\psi_{R0}\|$  is the magnitude of the operating-point rotor flux. It can be noticed that the poles  $s = -\omega_{rb} \pm j\omega_{r0}$  of (14) match with the open-loop poles of the rotor-flux dynamics driven by the stator flux [10].<sup>2</sup> These poles are stable, but they cannot be affected by means of the state-feedback control law (5). However, the damping of the poles can be increased via the stator frequency, as will be presented subsequently.

It is easy to show that  $\text{Re}\{G(j\omega)\} > 0$  holds for all  $\omega$  if  $|\omega_{r0}| < \omega_{rb}$  and  $\psi_{R0} > 0$ . Consequently, the transfer function  $G(s)$  is strictly passive in the whole feasible operating region. Its feedback interconnection with any passive mechanical subsystem remains passive, which indicates robustness for unknown mechanical subsystems. This complete passivity is a highly desirable property that cannot be achieved using conventional V/Hz control [2].

Next, the effect of the damping loop via the high-pass filter  $F(s)$  is considered. As shown in Appendix B, the torque estimation error is decoupled from the mechanical dynamics. Furthermore, the high-pass filter  $F(s)$  defined in (8) is passive. Therefore, the complete passivity (and stability) of the whole interconnected system shown in Fig. 3 is guaranteed for any passive mechanics [11].

To better understand the effect of the damping loop, a static gain  $F(s)$  can be considered. In this special case, the feedback interconnection of (14) and  $F(s) = k_\omega$  results in the system,

<sup>2</sup>Some readers might be familiar with the stator transient time constant  $T'_s = R_s/L_\sigma$  and the rotor transient time constant  $T'_r = 1/\omega_{rb}$  [10]. As a special case, choosing  $\sigma_c = R_s/L_\sigma$  results in the decoupled dynamics, where the decay rates correspond to the inverses of these transient time constants.

TABLE I  
DATA OF THE 2.2-KW FOUR-POLE INDUCTION MOTOR

Rated values		
Voltage (line-to-neutral, peak value)	$\sqrt{2/3} \cdot 400$ V	1 p.u.
Current (peak value)	$\sqrt{2} \cdot 5$ A	1 p.u.
Frequency	50 Hz	1 p.u.
Speed	1 430 r/min	0.95 p.u.
Torque	14.6 Nm	0.66 p.u.
Parameters		
Stator resistance $R_s$	3.7 $\Omega$	0.080 p.u.
Rotor resistance $R_R$	2.1 $\Omega$	0.045 p.u.
Leakage inductance $L_\sigma$	21 mH	0.143 p.u.
Magnetizing inductance $L_M$	224 mH	1.524 p.u.
Total inertia $J_m$	0.0155 kgm <sup>2</sup>	67.1 p.u.

whose denominator is  $(s + \omega_{rb})^2 + \omega_{r0}^2 + k_\omega(\omega_{rb}s + \omega_{rb}^2 + \omega_{r0}^2)$  and numerator remains the same as in (14). It can be seen that the damping is increased due to the term  $k_\omega\omega_{rb}s$ . In practice, the high-pass filter according to (8) is preferred over the static gain to avoid the steady-state speed error.

### C. Design Guidelines

The state-feedback gain matrix in the control law (5) could be chosen as  $\mathbf{K} = \sigma_c \mathbf{I} - \omega_{s0} \mathbf{J}$ , resulting in  $\mathbf{G}_c(s) = \sigma_c / (s + \sigma_c) \mathbf{I}$ , where the  $d$ - and  $q$ -axes dynamics are decoupled. However, this decoupling is unnecessary, and a simpler choice

$$\mathbf{K} = \sigma_c \mathbf{I} \quad (15)$$

is adopted here, where  $\sigma_c$  approximately corresponds to the closed-loop bandwidth. Since the natural frequency is not altered, the robustness against parameter errors is slightly better than in the case of the  $dq$ -decoupled design.

The decay rate for the observer gain in (12) can be scheduled as

$$\sigma_o = \zeta_\infty |\omega_s| + \alpha/2 \quad (16)$$

where  $\zeta_\infty$  is the desired damping ratio at high speeds. At zero stator frequency  $\omega_{s0} = 0$ , the poles are located at  $s = 0$  and  $s = -\alpha$ , which allows magnetizing and starting the motor in a stable manner. If both poles were placed at  $s = 0$ , the system would be unstable in the starting condition, which is a typical problem in conventional V/Hz control as well as in sensorless control if the observer gain is not well designed. At high speeds, the choice (16) results in the poles located at  $s = -(\zeta_\infty \pm j\sqrt{1 - \zeta_\infty^2})|\omega_{s0}|$ . Studying the pole locations and the resulting observer equations in more detail reveals that the choice (16) makes the observer dynamics to vary from the current-model-type dynamics (for the magnitude of the estimate) to well-damped voltage-model-type dynamics as the frequency increases from zero.

## V. RESULTS

The proposed observer-based V/Hz control method is studied by means of simulations and experiments. A 2.2-kW four-pole induction motor is used as an example motor. Its rated values and parameters are given in Table I.

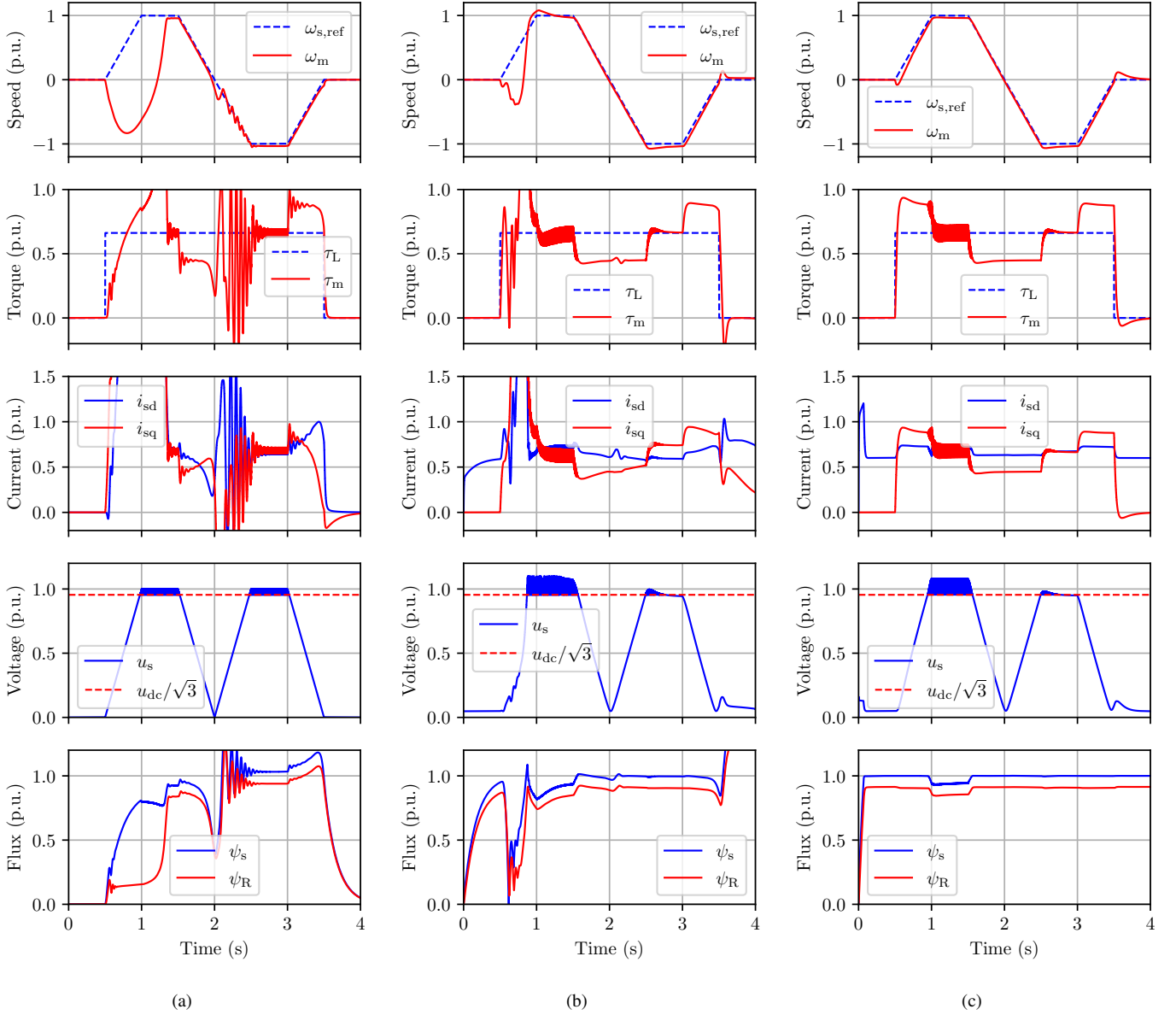


Fig. 4. Simulation results: (a) open-loop V/Hz control; (b) conventional V/Hz control with RI compensation and current-feedback-based compensator; (c) proposed observer-based V/Hz control. The speed reference is ramped:  $0 \rightarrow 1$  p.u.  $\rightarrow -1$  p.u.  $\rightarrow 0$ . The load torque increases stepwise from zero to its rated value (0.66 p.u.) in the beginning of the acceleration at  $t = 0.5$  s and decreases stepwise back to zero at  $t = 3.5$  s.

The variant (6) of the proposed control law is used. The state-feedback gain is selected according to (15) with  $\sigma_c = 2\pi \cdot 20$  rad/s. The bandwidth of the high-pass filter  $F(s)$  is  $\alpha_f = 2\pi \cdot 1$  rad/s and the damping gain is  $k_\omega = 3$  (Nm·s) $^{-1}$ . The design parameters for the observer are  $\zeta_\infty = 0.7$  and  $\alpha_o = 2\pi \cdot 40$  rad/s. It is to be noted that the choice of these design parameters is not critical, i.e., they could be varied in a wide range. The slip compensation is disabled.

#### A. Simulations

The proposed observer-based V/Hz control is studied with simulations by comparing it to conventional V/Hz control. Fig. 4 shows simulation results for three different controllers:

- (a) Open-loop V/Hz control [Fig. 1(a), with  $C(s) = \mathbf{0}$  and  $F(s) = 0$ ];
- (b) Conventional V/Hz control [Fig. 1(a), parametrized as described in Appendix A].
- (c) Proposed observer-based V/Hz control [Fig. 1(b)].

In Fig. 4, the frequency reference is ramped from zero to the rated frequency, then reversed, and finally ramped back to zero. The load torque increases stepwise from zero to its rated value (0.66 p.u.) in the beginning of the acceleration. When the frequency reference finally reaches zero at the end of the sequence, the load torque decreases stepwise to zero.

Fig. 4(a) shows results for open-loop V/Hz control. During almost the whole sequence, the system is either unstable or

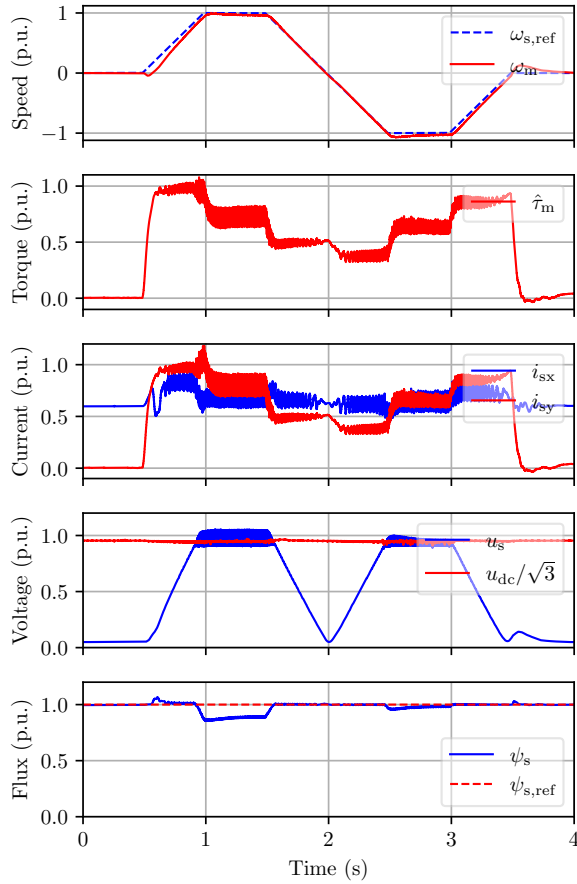


Fig. 5. Experimental results for the proposed observer-based V/Hz control, corresponding to the simulation results shown in Fig. 4(c).

poorly damped. Fig. 4(b) shows results for conventional V/Hz control with RI compensation (perfectly parameterized) and current-feedback-based compensator. It can be seen that the system is unstable in the beginning of the acceleration (due to the flux collapse) as well as at the end of the sequence (due to the flux surge). Signs of instability can also be seen while crossing the zero frequency in the middle of the sequence. The noise in the currents at the frequency of 1 p.u. originates from the overmodulation, as can be also seen from the waveform  $u_s$  of the voltage magnitude. The waveform  $u_{dc}/\sqrt{3}$  of the scaled DC-link voltage shows the limit of the linear modulation region.

Fig. 4(c) shows simulation results for proposed observer-based V/Hz control. As expected, the system is stable and well damped. The magnetization is fast and well damped, corresponding to the desired stator-flux dynamics.

### B. Experiments

The experiments were conducted on the proposed control method using a dSPACE MicroLabBox prototyping unit. The same design parameters were used as in the simulations. The switching frequency was 4 kHz, and the inverter nonlinearities were compensated for using a current feed-forward method

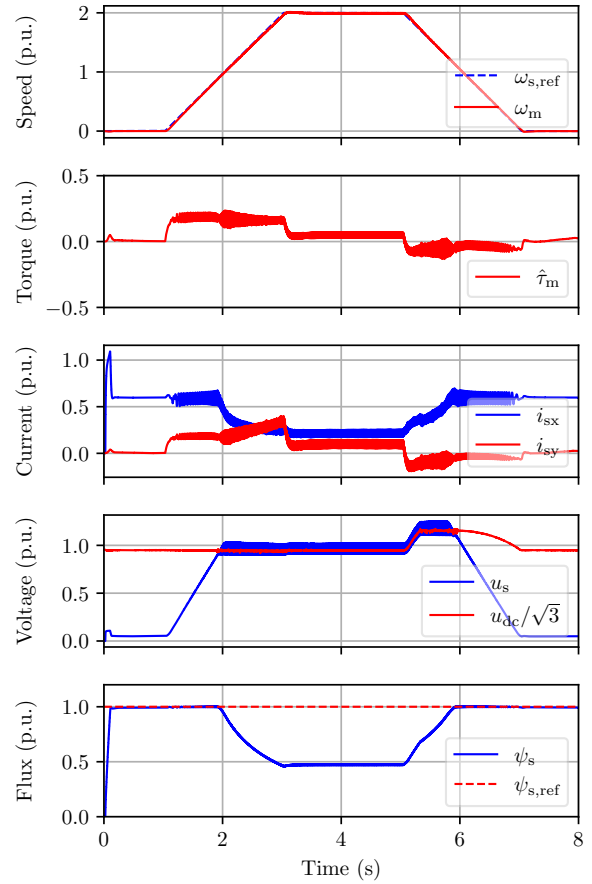


Fig. 6. Experimental results showing field-weakening operation. The stator frequency reference is ramped:  $0 \rightarrow 2$  p.u.  $\rightarrow 0$ . No load torque is applied.

[12]. The rotor speed was measured using a resolver for monitoring purposes.

Fig. 5 shows results corresponding to the simulation sequence in Fig. 4(c). It can be seen that the measurement results match with the simulations results well. It is to be noted that the chosen sequence is particularly difficult for speed sensorless control methods due to the stepwise change of load torque at zero speed and slow speed reversal while loaded.

Fig. 6 shows experimental results of the field-weakening operation. The frequency reference is ramped from zero to 2 p.u. and the load torque is zero. The control method automatically handles field-weakening when the maximum inverter voltage is reached (even if the constant flux reference  $\psi_{s,ref} = 1$  p.u. is used). The sequence also shows that the motor is magnetized in a stable manner in the beginning of the sequence. After  $t = 5$  s, the DC-link voltage rises due to regenerative braking during deceleration. A braking chopper limits the DC-link voltage from rising excessively.

Fig. 7 shows experimental results where the frequency reference is first ramped from zero to 0.5 p.u. and then the load torque is increased stepwise from zero to its rated value

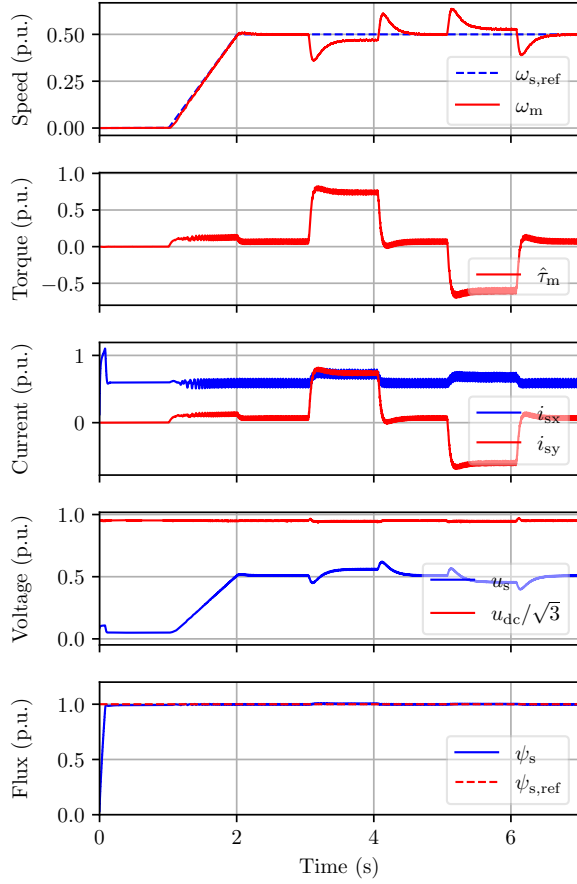


Fig. 7. Experimental results showing the acceleration from 0 to 0.5 p.u. as well as the rated positive and negative load torque steps.

and back to zero, followed by a similar load torque step with negative sign. It can be seen that the response is well damped.

## VI. CONCLUSIONS

The proposed observer-based V/Hz control has a simple structure, closely resembling conventional V/Hz control. The proposed method contains no speed controller, which simplifies the tuning of the control system. Furthermore, field weakening is inherent to the method without a separate algorithm. The method also allows full utilization of the inverter voltage since no voltage margin is needed. The method is completely stable and passive, and, consequently, robust against unknown mechanics. As compared to heuristic V/Hz control structures, a trial-and-error process in tuning can be reduced since all the design parameters have a clear physical meaning.

### APPENDIX A CONVENTIONAL V/Hz CONTROL

Fig. 1(a) shows a conventional V/Hz control system. The voltage reference is

$$\mathbf{u}_{s,\text{ref}} = \omega_s \mathbf{J} \psi_{s,\text{ref}} + \mathbf{C}(s) \mathbf{i}_s \quad (17)$$

where the compensator  $\mathbf{C}(s)$  is described by a  $2 \times 2$  transfer-function matrix. Typically, this compensator consists of parallel connection of RI compensation and high-pass filtering in order to improve damping in the mid-speed region [2], [4]. An example compensator is constructed as

$$\mathbf{C}(s) = \underbrace{\frac{\alpha_1}{s + \alpha_1} R_s \mathbf{I}}_{\text{RI compensation}} + \underbrace{\frac{s}{s + \alpha_2} k_u L_\sigma \omega_s \mathbf{J}}_{\text{Damping}} \quad (18)$$

where  $k_u$  is a positive gain, and  $\alpha_1$  and  $\alpha_2$  are low- and high-pass filter bandwidths, respectively. The torque estimate is based on the measured current and the flux reference,

$$\hat{\tau}'_m = \mathbf{i}'_s{}^T \mathbf{J} \psi_{s,\text{ref}} \quad (19)$$

Alternatively, the damping via the stator frequency could be implemented based on the estimated slip frequency [2].

For the simulations of this paper, the compensator  $\mathbf{C}(s)$  is parametrized with  $k_u = 1$  and  $\alpha_1 = \alpha_2 = 0.1\omega_{rb}$ . The bandwidth of the high-pass filter  $F(s)$  is  $\alpha_f = 2\pi \cdot 1 \text{ rad/s}$  and the damping gain is  $k_\omega = 3 \text{ (Nm}\cdot\text{s)}^{-1}$ .

### APPENDIX B LINEARIZED MODEL

*Motor Model:* Linearizing the induction motor model in (1) yields [2]

$$\begin{aligned} \frac{d\Delta\mathbf{x}}{dt} = & \underbrace{\begin{bmatrix} -\frac{R_\sigma}{L_\sigma} \mathbf{I} - \omega_{s0} \mathbf{J} & \frac{1}{L_\sigma} (\alpha \mathbf{I} - \omega_{m0} \mathbf{J}) \\ R_R \mathbf{I} & -\alpha \mathbf{I} - \omega_r \mathbf{J} \end{bmatrix}}_A \Delta\mathbf{x} \\ & + \underbrace{\begin{bmatrix} \frac{1}{L_\sigma} \mathbf{I} \\ \mathbf{0} \end{bmatrix}}_B \Delta\mathbf{u}_s + \underbrace{\begin{bmatrix} -\mathbf{J} \mathbf{i}_{s0} \\ -\mathbf{J} \psi_{R0} \end{bmatrix}}_c \Delta\omega_s - \underbrace{\begin{bmatrix} \frac{1}{L_\sigma} \mathbf{J} \psi_{R0} \\ -\mathbf{J} \psi_{R0} \end{bmatrix}}_b \Delta\omega_m \end{aligned} \quad (20a)$$

where  $\Delta\mathbf{x} = [\Delta\mathbf{i}'_s{}^T, \Delta\psi_{R0}^T]^T$  is the state vector. The linearized output equations are

$$\Delta\psi_s = \underbrace{[L_\sigma \mathbf{I} \quad \mathbf{I}]}_C \Delta\mathbf{x} \quad (20b)$$

$$\Delta\tau_m = \underbrace{[-\psi_{R0}^T \mathbf{J} \quad \mathbf{i}'_{s0}{}^T \mathbf{J}]}_{c^T} \Delta\mathbf{x} \quad (20c)$$

The operating-point stator current appearing in the linearized model can be written as a function of the rotor flux and the slip frequency using (3).

*State-Feedback Control:* Accurate parameter estimates will be assumed. The control law (5) is linearized, resulting in

$$\Delta\mathbf{u}_s = -\mathbf{K}_c \Delta\mathbf{x} + \mathbf{K} \Delta\tilde{\psi}_R + \mathbf{N} \Delta\psi_{s,\text{ref}} + \mathbf{J} \psi_{s0} \Delta\omega_s \quad (21)$$

where  $\Delta\tilde{\psi}_R = \Delta\psi_R - \Delta\hat{\psi}_R$  is the flux estimation error,  $\mathbf{K}_c = [L_\sigma \mathbf{K} - R_s \mathbf{I}, \mathbf{K}]$  is the state-feedback gain matrix and  $\mathbf{N} = \omega_{s0} \mathbf{J} + \mathbf{K}$  is the reference-feedforward gain matrix. Inserting (21) into (20) results in the closed-loop system

$$\frac{d\Delta\mathbf{x}}{dt} = \mathbf{A}_c \Delta\mathbf{x} + \mathbf{B} \mathbf{K} \Delta\tilde{\psi}_R + \mathbf{B} \mathbf{N} \Delta\psi_{s,\text{ref}} + \mathbf{b} \Delta\omega_s \quad (22)$$

where  $\mathbf{A}_c = \mathbf{A} - \mathbf{B}\mathbf{K}_c$  and  $\Delta\omega_\delta = \Delta\omega_s - \Delta\omega_m$ . As will be shown subsequently, the separation principle holds for the linearized control and observer dynamics. Therefore, the transfer functions (13) and (14), respectively, can be calculated using the state-space matrices as

$$\mathbf{G}_c(s) = \mathbf{C}(s\mathbf{I}_4 - \mathbf{A}_c)^{-1}\mathbf{B}\mathbf{N} \quad (23a)$$

$$G(s) = \mathbf{c}^T(s\mathbf{I}_4 - \mathbf{A}_c)^{-1}\mathbf{b} \quad (23b)$$

Furthermore, the control characteristic polynomial is  $D_c(s) = \det(s\mathbf{I}_4 - \mathbf{A}_c) = [(s + \sigma_c)^2 + \omega_d^2][(s + \omega_{rb})^2 + \omega_{r0}^2]$ .

*Reduced-Order Flux Observer:* The reduced-order observer (11) is linearized. Using (20), the resulting dynamics can be expressed as [6]

$$\begin{aligned} \frac{d\Delta\tilde{\psi}_R}{dt} = & \underbrace{-[\omega_{s0}\mathbf{J} + \mathbf{K}_o(\alpha\mathbf{I} - \omega_{m0}\mathbf{J})]}_{\mathbf{A}_o} \Delta\tilde{\psi}_R \\ & + \underbrace{\mathbf{K}_o\mathbf{J}\psi_{R0}}_{\mathbf{b}_o} \Delta\tilde{\omega}_m \end{aligned} \quad (24a)$$

$$\frac{d\Delta\hat{\omega}_m}{dt} = \underbrace{\frac{\alpha_o\psi_{R0}^T\mathbf{J}(\alpha\mathbf{I} - \omega_{m0}\mathbf{J})}{\psi_{R0}^2}}_{\alpha_o^T} \Delta\tilde{\psi}_R + \alpha_o\Delta\tilde{\omega}_m \quad (24b)$$

$$\Delta\tilde{\psi}_s = \Delta\tilde{\psi}_R \quad (24c)$$

$$\Delta\tilde{\tau}_m = \dot{\mathbf{i}}_{s0}^T\mathbf{J}\Delta\tilde{\psi}_R \quad (24d)$$

where  $\Delta\tilde{\omega}_m = \Delta\omega_m - \Delta\hat{\omega}_m$ . The observer gain, corresponding to (12), resulting from the linearization procedure is

$$\mathbf{K}_o = \frac{2\sigma_o(\alpha\mathbf{I} + \omega_{m0}\mathbf{J})}{\alpha^2 + \omega_{m0}^2} \frac{\psi_{R0}\psi_{R0}^T}{\psi_{R0}^2} \quad (25)$$

Since  $\mathbf{b}_o = \mathbf{0}_{2,1}$  holds for this gain, the flux and torque estimation dynamics are decoupled from the speed estimate as well as from the speed input  $\Delta\omega_m$ . The observer characteristic polynomial is  $D_o(s) = (s^2 + 2\sigma_o s + \omega_{s0}^2)(s + \alpha_o)$ . It is also to be noted that the speed estimate  $\hat{\omega}_m$  appearing in the observer gain (12) introduces no coupling in the linearized model since the operating-point estimation errors are zero under the assumption of accurate parameter estimates.

*Separation Principle:* To show the validity of the separation principle, the closed-loop system including the observer is also presented. As mentioned,  $\mathbf{b}_o = \mathbf{0}_{2,1}$  holds for inherently sensorless observers. Combining the control and observer dynamics yields

$$\begin{aligned} \frac{d\Delta\mathbf{z}}{dt} = & \underbrace{\begin{bmatrix} \mathbf{A}_c & \mathbf{B}\mathbf{K} & \mathbf{0}_{4,1} \\ \mathbf{0}_{2,4} & \mathbf{A}_o & \mathbf{0}_{2,1} \\ \mathbf{0}_{1,4} & \mathbf{a}_o^T & -\alpha_o \end{bmatrix}}_{\mathbf{A}_t} \Delta\mathbf{z} + \begin{bmatrix} \mathbf{B}\mathbf{N} \\ \mathbf{0} \\ \mathbf{0}_{1,2} \end{bmatrix} \Delta\psi_{s,\text{ref}} \\ & + \begin{bmatrix} \mathbf{b} \\ \mathbf{0}_{2,1} \\ 0 \end{bmatrix} \Delta\omega_\delta + \begin{bmatrix} \mathbf{0}_{4,1} \\ \mathbf{0}_{2,1} \\ \alpha_o \end{bmatrix} \Delta\omega_m \end{aligned} \quad (26a)$$

where  $\Delta\mathbf{z} = [\Delta\mathbf{x}^T, \Delta\tilde{\psi}_R^T, \Delta\hat{\omega}_m]^T$  is the augmented state vector. As an example, applying (20) and (24), the following linearized output equations are obtained

$$\Delta\hat{\psi}_s = [\mathbf{C} \quad -\mathbf{I} \quad \mathbf{0}_{2,1}] \Delta\mathbf{z} \quad (26b)$$

$$\Delta\hat{\tau}_m = [\mathbf{c}^T \quad -\dot{\mathbf{i}}_{s0}^T\mathbf{J} \quad 0] \Delta\mathbf{z} \quad (26c)$$

The resulting transfer functions from the inputs to these estimates are the same as those without the observer dynamics. Due to the zero blocks of  $\mathbf{A}_t$ , the separation principle holds as expected, i.e., the characteristic polynomial is  $D_t(s) = \det(s\mathbf{I}_7 - \mathbf{A}_t) = D_c(s)D_o(s)$ .

## REFERENCES

- [1] R. H. Nelson, T. A. Lipo, and P. C. Krause, "Stability analysis of a symmetrical induction machine," *IEEE Trans. Power App. Syst.*, vol. PAS-88, no. 11, pp. 1710–1717, Nov. 1969.
- [2] M. Hinkkanen, L. Tiitinen, E. Mölsä, and L. Harnefors, "On the stability of volts-per-hertz control for induction motors," *IEEE Trans. Emerg. Sel. Topics Power Electron.*, vol. 10, no. 2, pp. 1609–1618, Apr. 2022.
- [3] A. Muñoz-García, T. A. Lipo, and D. W. Novotny, "A new induction motor V/f control method capable of high-performance regulation at low speeds," *IEEE Trans. Ind. Appl.*, vol. 34, no. 4, pp. 813–821, Jul./Aug. 1998.
- [4] G.-J. Jo and J.-W. Choi, "Rotor field-oriented V/f drive system implementation with oscillation suppression compensator in induction motors," *IEEE Trans. Emerg. Sel. Topics Power Electron.*, vol. 9, no. 3, pp. 2745–2758, Jun. 2021.
- [5] L. Harnefors and M. Hinkkanen, "Complete stability of reduced-order and full-order observers for sensorless IM drives," *IEEE Trans. Ind. Electron.*, vol. 55, no. 3, pp. 1319–1329, 2008.
- [6] M. Hinkkanen, L. Harnefors, and J. Luomi, "Reduced-order flux observers with stator-resistance adaptation for speed-sensorless induction motor drives," *IEEE Trans. Power Electron.*, vol. 25, no. 5, pp. 1173–1183, May 2010.
- [7] G. R. Slemon, "Modelling of induction machines for electric drives," *IEEE Trans. Ind. Appl.*, vol. 25, no. 6, pp. 1126–1131, Nov./Dec. 1989.
- [8] L. Harnefors, "Design and analysis of general rotor-flux-oriented vector control systems," *IEEE Trans. Ind. Electron.*, vol. 48, no. 2, pp. 383–390, 2001.
- [9] G. C. Verghese and S. R. Sanders, "Observers for flux estimation in induction machines," *IEEE Trans. Ind. Electron.*, vol. 35, no. 1, pp. 85–94, Feb. 1988.
- [10] J. Holtz, "On the spatial propagation of transient magnetic fields in ac machines," *IEEE Trans. Ind. Appl.*, vol. 32, no. 4, pp. 927–937, Jul./Aug. 1996.
- [11] H. K. Khalil, *Nonlinear systems*, 2nd ed. Upper Saddle River, NJ: Prentice-Hall, 1996.
- [12] J.-W. Choi and S.-K. Sul, "Inverter output voltage synthesis using novel dead time compensation," *IEEE Trans. Power Electron.*, vol. 11, no. 2, pp. 221–227, 1996.